ISSN 0020-4412, Instruments and Experimental Techniques, 2006, Vol. 49, No. 1, pp. 83–91. © Pleiades Publishing, Inc., 2006.
Original Russian Text © A.V. Bubley, V.M. Panasyuk, V.V. Parkhomchuk, V.B. Reva, 2006, published in Pribory i Tekhnika Eksperimenta, 2006, No. 1, pp. 91–99.

GENERAL EXPERIMENTAL TECHNIQUES

Measurements of the Profile of an Intense Electron Beam

A. V. Bubley, V. M. Panasyuk, V. V. Parkhomchuk, and V. B. Reva

Budker Institute for Nuclear Physics, Siberian Division, Russian Academy of Sciences, pr. Akademika Lavrent'eva 11, Novosibirsk, 630090 Russia

Received April 29, 2005

Abstract—Methods for measuring the profiles of high-power electron beams by using a thin tungsten wire moved transversely to the beam have been developed. In one method, the electron current intercepted by the wire is measured and the beam profile is determined from a solution to the Abel equation under the assumption of axial beam symmetry. The second method is based on the detection of the local radiation emitted by the wire being heated by the beam to 1700–2200 K. The wire is additionally heated by an electric current in order to improve the sensitivity and spatial resolution. The measured beam current density is ~5–50 A/cm^2, and the resolution is ~0.1 cm.

PACS numbers: 07.77.Ka, 29.27.Fh, 29.27.Bd, 29.20.Dh

DOI: 10.1134/S0020441206010106

INTRODUCTION

Cooling of an ion beam by an accompanying cold-electron beam is a widespread technique in accelerator physics [1]. This method was tested for the first time in 1974 in Novosibirsk [2] and is now one of the basic techniques for achieving high phase density of ion beams in storage rings. Even transitions of ultracold beams to an internally ordered state were discovered in experiments, this stimulating the development of a special field in accelerator physics—the physics of crystal beams. However, at high current densities, the development of coherent instabilities was observed on a number of facilities and led to problems arising with beam stacking. In addition, in some cases, recombination of ions at electrons of the cooling beam became considerable.

One of the methods for solving the aforementioned problems is the production of an electron beam with a specified radial profile. The cooling intensity is directly proportional to the electron density and inversely proportional to the cubed amplitude of the betatron oscillations of ions. Hence, by reducing the density of an electron beam at its center, it is possible to substantially suppress the recombination process and undesirable collective ion–electron interaction by slightly reducing the cooling time.

Using an electron beam with a variable profile, it is also possible to realize additional opportunities in accelerator experiments, for example, either to hold the ion-beam size within preset limits without permitting a large shift of the frequency of betatron oscillations on the space charge or to cool to the highest degree the central part of the ion beam during its interaction with an internal target.

To solve these problems, we have developed an electron gun with a controlled beam profile [3, 4]. The operational features of this electron gun were studied and the beam profiles in different operating modes were measured on a special gun–collector setup at the Institute of Nuclear Physics, Siberian Division, Russian Academy of Sciences. The results of these measurements are presented below.

MEASUREMENT TECHNIQUE

A thin tungsten wire moved by a stepping motor transversely to the beam was used to measure the electron-beam profile. The beam profile was measured by two methods.

The first method involved measurements of the current of electrons incident on the wire. Operating under the assumption of axial beam symmetry, the beam-current density distribution $j_e(r)$ can be found from the solution of the Abel equation:

$$J_e(y^2) = d\int_{y^2}^{R^2} j_e(r^2)\frac{dr^2}{\sqrt{r^2 - y^2}}, \quad (1)$$

where d is the wire diameter (20 μm), R is the outer beam radius (1.5 cm), r is the current beam radius, y is the coordinate of the chord from the beam center along the line of motion, and $J_e(y^2)$ is the measured coordinate dependence of the current from the wire. Measurements were performed in a strong external magnetic field, and it was therefore assumed that secondary electrons fall on the wire.

In the second method, local measurements of radiation from the current-heated wire were performed. In

each position of the wire, a special photodetector scanned the longitudinal distribution of the wire glow.

The profile $Q(x)$ of the beam power density along the wire is generally related to the emission density via the equation

$$-\pi a^2\left[\frac{d}{dx}\left(\chi(T)\frac{dT}{dx}\right)\right] = \frac{j_h^2}{\pi a^2}\rho(T) + 2aQ(x) - 2\pi a q(T), \quad (2)$$

where $T(x)$ is the temperature profile along the chord, x is the current coordinate along the chord, J_h is the filament current in the wire, $\rho(T)$ is the tungsten resistivity, $q(T)$ is the emitted power density, and $\chi(T)$ is the thermal conductivity for tungsten.

This equation considers the following effects: the heat transfer to the wire ends owing to heat conduction (the left-hand side of Eq. (2)), the heat inflow due to heating by an external current (the first term on the right-hand part), the wire heating by the beam's electron current (the second term on the right-hand part), and the power emission through the glow (the third term on the right-hand part).

The wire was heated by an external current with a known power for calibrating the emission-power meter and improving the dynamic range of photodetectors in beam-profile measurements. In addition, the wire heating contributes to an increase in the spatial resolution, since the fraction of radiation losses (the valid signal) increases in comparison with the heat losses through conduction.

In a general case, the beam-profile reconstruction requires the knowledge of dependence $T(S)$, where S is a photodetector signal. The profile of $S(x)$ must be measured with the maximum possible spatial resolution because of the necessity of its subsequent differentiation during processing.

Figure 1 shows a schematic of the gun–collector setup for measuring the beam profile. Its magnetic system consists of two solenoids *3* and *4* mounted vertically. Gun *2* is placed in the bottom part and inserted into the lower solenoid to a depth of ~7.5 cm. Magnetic-flux concentrator *5* made of iron is used to create a magnetic field in the region of the gun cathode. Collector *1*, being situated inside a field-forming shield, is placed 1 cm higher than the upper solenoid. The distance between the gun and the collector is ~110 cm. The solenoids are powered independently, thus allowing the beam size to be varied at the collector input. The magnetic fields change in the range 0.3–0.7 kG. The gap between the solenoids (~20 cm) was used for pumping and for diagnostic purposes. The vacuum chamber has the form of 3D cross-type system *7*, along the vertical tube of which a beam propagates. The arrangement of instruments on the horizontal tubes is shown in the diagram of the system for beam-profile measurements (Fig. 2).

A tungsten wire 20 μm in diameter and 10 cm in length is tensioned through insulators on a spring-type metal frame fixed on a movable rod (see Fig. 2). This structure is situated inside the vacuum chamber. The wire ends are led out through a ceramic connector. The rod is moved perpendicularly to the beam direction by stepping motor via bellows *5*.

The radiation emitted by the incandescent tungsten filament was extracted through vacuum glass window *3*. Photodiode *1* with an OPT211 amplifier was installed inside Зенит-ET camera *2* equipped with a standard Гелиос-44 lens and a slit diaphragm and served as a photodetector. The optical system's spatial resolution in length was 0.5 mm. The camera was fixed on a scanner that, using an electric motor, underwent vibrations in a horizontal plane. The total angular magnitude was 10° at an arm of ~100 cm and allowed viewing of the entire wire length with a margin. At each step, the wire length was scanned five times, and 100 readings of signals from the photodiode and the coordinate detector were taken in each scan.

Since the emission power greatly increases with the temperature, the wire must have a high temperature. The maximum operating temperature of tungsten in vacuum is 2800 K [6], but the evaporation of tungsten at this temperature is appreciable. In this case, an acceptable temperature of the W wire is 2200 K, at which the saturation vapor pressure is 7.4×10^{-10} torr. The corresponding emission power density is q = 37 W/cm^2, from which an estimate of the tolerable local beam-power density follows: $Q \approx \pi q \approx 120$ W/cm^2. At T = 2200 K, the radiation peak lies at a wavelength $\lambda_m \approx 1.3$ μm.

The first measurement run was performed with comparatively weak stationary beams with an electron energy of 1 keV and currents of up to 0.17 A. The beam radius was 1.5 cm, and the power density averaged over the beam cross section was as high as ~24 W/cm^2.

In the second run, the gun operated in the rated mode. Beams with currents of up to 2.4 A and electron energies of up to 5 keV were formed. The subsequent use of such beams for cooling ions only requires their acceleration. In a stationary beam with a cross-section averaged power density of ~1.7 kW/cm^2, the wire burns away; therefore, a periodic sequence of enabling (τ = 0.28 ms) and blanking pulses was fed to the gun's control electrode. The average value of the beam-power density was then 40 W/cm^2, which corresponded to an average temperature of the wire of ~1770 K. The thermal skin layer $(4k\tau)^{1/2} = 1.7 \times 10^{-2}$ cm, where k = 0.25 cm^2/s is the thermal diffusivity for tungsten, exceeds the wire diameter by an order of magnitude; consequently, the wire was heated throughout its entire cross section in each pulse. The temperature increment per pulse at a power density of 1.7 kW/cm^2 was 80 K, which was the magnitude of the temperature oscillations against the background of the average value.

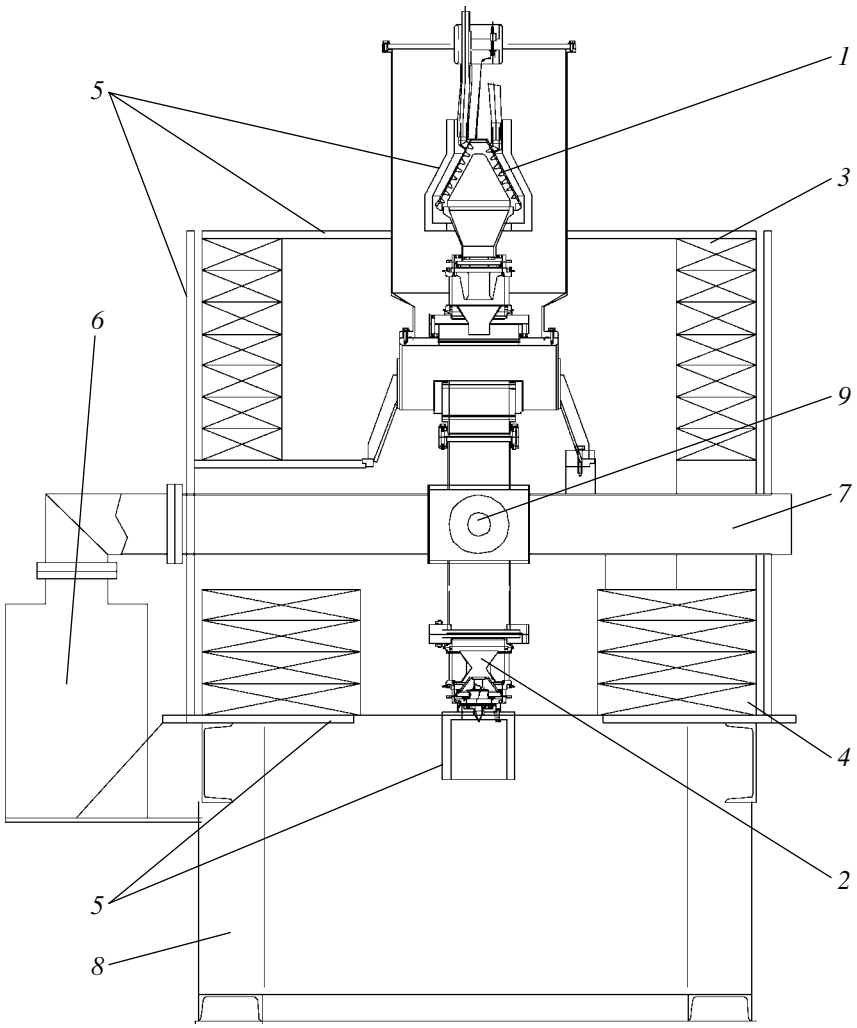

Fig. 1. Schematic of the gun–collector setup: (*1*) collector, (*2*) electron gun with a variable beam profile, (*3*) coils of the collector's magnetic system, (*4*) coils of the gun's magnetic system, (*5*) magnetic circuits and magnetic-flux concentrators, (*6*) ion pump, (*7*) cross-type system for evacuation (one arm) and insertion of a probe (the other arm), (*8*) bearing structure of the setup, and (*9*) viewing window of the vacuum system.

The estimates of the average heat load on the wire presented above are several times lower than the tolerable load. However, the local power density of hollow or parabolic beams is several times higher than the average one and the local heating of the wire is correspondingly higher.

CALIBRATION WITH A DIRECT CURRENT

The calibration involved scanning along the entire wire length accompanied by step-by-step recording of the coordinate dependence of the signal from the photodiode at 14 values of filament current J_k. Some of the measured dependences are presented in Fig. 3a. It is seen that, in almost all measurements along the wire, the signal from the photodiode is nearly constant. Hence, almost the entire absorbed energy was radiated. The longitudinal heat conduction that competed with radiation manifested itself noticeably at the wire edges only at low filament currents (lower curves).

A regular nonuniformity of signals at $x = -3.4$ cm may be related to a locally thickened wire section. According to estimates, the change in the signal observed in all measurements corresponds to a local increase in the wire diameter of ~1.5 μm. Another possible explanation is a local decrease in the radiating capacity owing to a nonuniform emissivity. Since this type of nonuniformity remained unchanged during the whole study, it can be taken into consideration quite easily during the processing of experimental data. The signals at $x < -5$ cm and $x > 5$ cm, which are usually smaller than a signal from the wire, are signals owing to the photodiode illumination by scattered radiation. At a signal level of $S < 10^{-3}$ mV, illumination from the cathode was already perceptible.

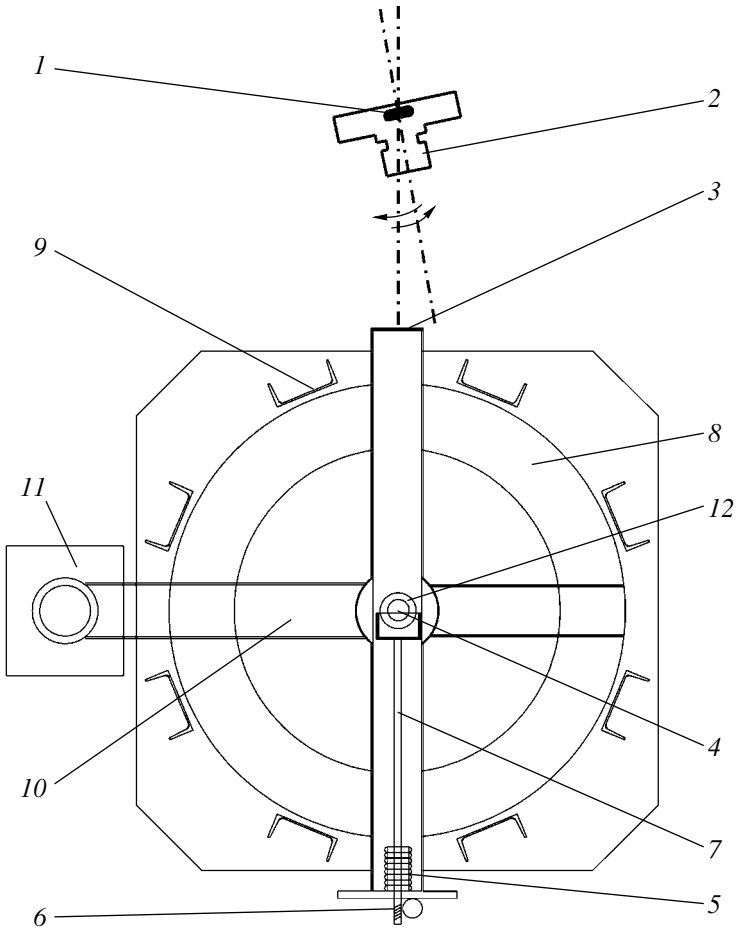

Fig. 2. System for measuring the beam profile: (*1*) photodiode, (*2*) Зенит-ET camera, (*3*) vacuum window, (*4*) tungsten wire, (*5*) bellows, (*6*) mechanical drive, (*7*) movable rod, (*8*) solenoid's winding, (*9*) parts of the magnetic circuit, (*10*) vacuum chamber, (*11*) ion pump, and (*12*) electron beam.

Figure 3b shows the signal from the wire's center as a function of filament-current power P_k. This dependence is close to a square law at $P_k > 0.1$ mW. Inverse dependence $q_k(S_k)$ allows profile $Q(x) = \pi q(x)$ of the beam-power density along the wire to be found from measured signal S_k in the case where the profile is smooth enough and the thermal conductivity along the wire can be ignored. Here, $q_k = P_k/(\pi dL)$ is the radiation-power density, $d = 19.2 \times 10^{-4}$ cm is the wire diameter, and $L = 10$ cm is the wire length.

Beams with steep boundaries can be reconstructed from measured signal $S(x)$ if the temperature dependence of photodetector signal S is known (see Eq. (2)). For this purpose, the temperature dependence of the tungsten resistivity, which is close to a linear function, can be used. Each of 14 measured values $\rho_k = \dfrac{U_k \pi d^2}{4 J_h L}$, where U_k is the filament voltage, corresponds to a reference temperature value T_k. Resulting dependence $S_k(T_k)$ is shown in Fig. 4a.

It is known that emissivity $\varepsilon(T) = q(T)/\sigma T^4$ strongly depends on the state of the surface. At the beginning, the wire-emitted glow was nonuniform and very bright at some places. Stable and reliable experimental data were obtained only some time later, after the entire surface of the wire had been exposed to an electron beam for a sufficiently long time and baked at maximum acceptable current values.

Calibration $q_k(S_k)$ and $T_k(S_k)$ was performed some time later after the wire surface had been completely cleaned and had attained an equilibrium state.

As a verification of this calibration, Fig. 4b shows the correspondence between measured dependence of radiation-power density $q_k(T_k)$ and reference function $q(T)$. Moreover, the values of photodetector signal $S(T_k)$ multiplied by constant C lie properly on curve $q_\lambda(T)$, which is the radiation-power density within the photodetector bandwidth normalized to its sensitivity. This curve is the product of $\varepsilon(T)$ by the integral with respect to the wavelength of the Plank's formula for blackbody emission multiplied by the photodetector's relative (normalized to unity) spectral sensitivity. The transmit-

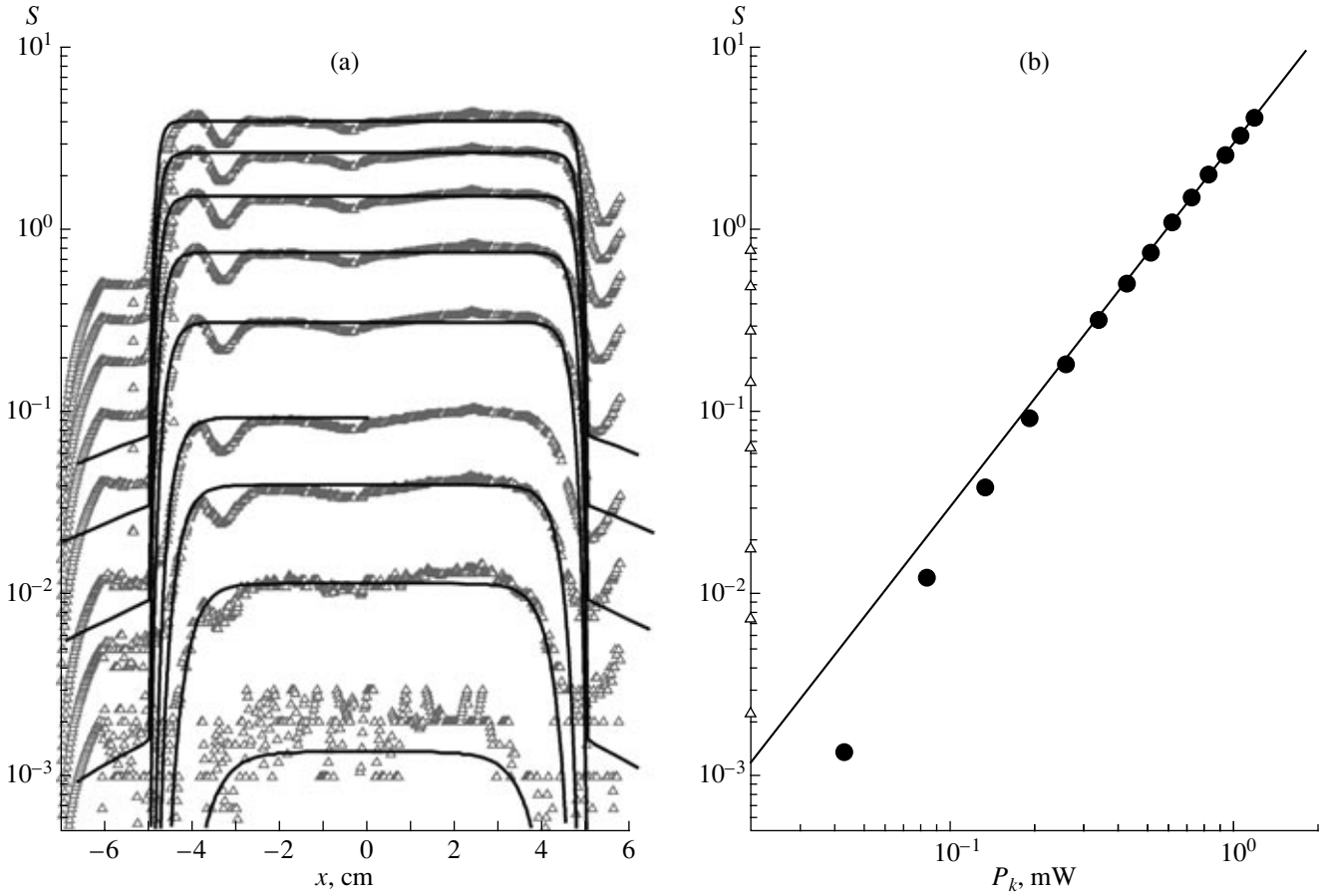

Fig. 3. (a) Profiles of photodiode signals at different values of the wire filament current (solid curves are the calculated signal profiles (see below)) and (b) signal as a function of the filament power.

tance of glass (the vacuum window and the lens) is approximately constant within the photodetector's sensitivity band.

Hence, the calibration results in two dependences. The first one is photodetector signal S as a function of emitted power density q obtained in direct measurements. If the beam profile is smooth enough and the thermal conductivity along the wire can be ignored, the profile can be easily determined using inverse dependence $q(S)$. The second dependence is photodetector signal S as a function of wire temperature T, which is necessary when the thermal conductivity along the wire cannot be ignored. This function results from the processing of measurements using reference data. The reliability of function $S(T)$ is confirmed only by the good coincidence of the reference and measured data shown in Figs. 4a and 4b. Pyrometric measurements could have been an alternative, but the coincidence of the true and brightness temperatures is also a reference issue. As was already mentioned, the beam-profile reconstruction requires not only inverse dependence $T(S)$, but its derivatives as well.

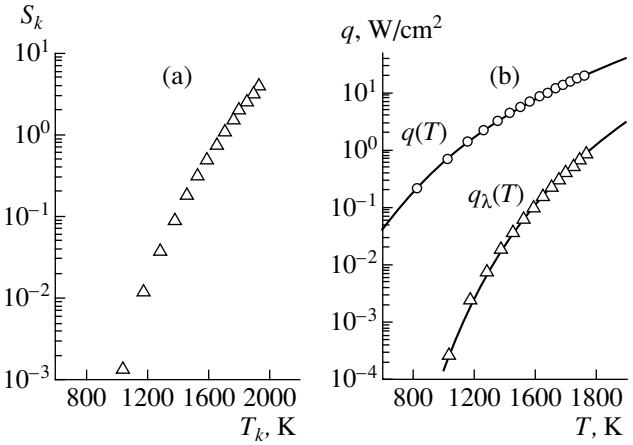

Fig. 4. (a) Photodiode signals S_k as a function of temperature T_k determined from the reference temperature dependence of resistivity $\rho(T)$. (b) Temperature dependence of the radiation-power density $q(T)$ (a solid curve and dots are the reference and measured values of $q_k(T_k)$, respectively) and temperature dependence of the radiation-power density $q_\lambda(T)$ within the photodetector bandwidth (a solid curve is the calculations, and dots are normalized values of photodetector signals).

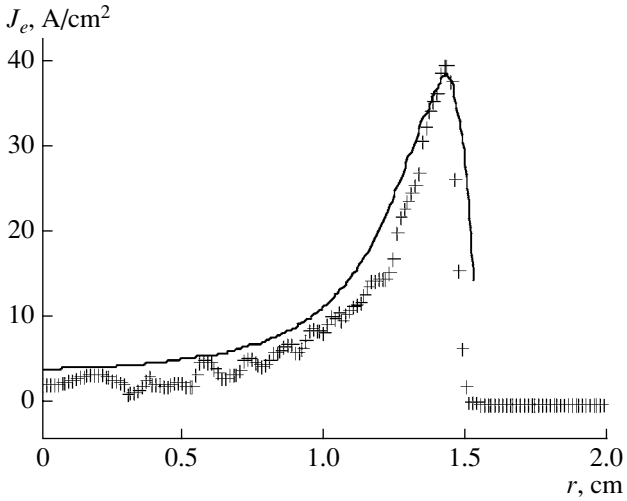

Fig. 5. Normalized beam profile (crosses) reconstructed from direct measurements of the current to the wire. The solid line is the result of a numerical simulation of the operating gun.

BEAM PROFILE MEASUREMENTS

Figure 5 shows the normalized profile of the beam-current density obtained from measurements of the current through the wire that is being displaced step by step transversely to the beam direction. The beam is assumed to be axially symmetrical, and the profile is a solution to Abel equation (1). Figure 5 also shows a profile that results from a numerical simulation using the SAM programs [3] for the gun operation at the same gun parameters.

Figure 6 shows the density distributions of the emitted power obtained during 2D electron-beam scanning in different operating modes of the gun. These distributions are presented in the form of frames in which each density value corresponds to a certain degree of brightness. Radiation was detected during scanning of the photodetector along the beam-crossing wire (from the left to the right in the frames); subsequently, the wire was displaced stepwise transversely to the beam direction (upward in the frames). For all frames, the gun cathode voltage was $U_{cath} = -1$ kV and the anode voltage was $U_a = 0.5$ kV. The beams' profiles were specified by a voltage U_{contr} applied to the control electrode relative to the cathode.

An azimuthal nonuniformity observed in the distributions is associated with the fact that, beginning with the second frame, the beam-power density is concentrated within a narrow layer at its outer boundary. The longitudinal thermal conductivity causes both the temperature profile and, as a consequence, the emitted power density to spread. In the upper and bottom parts, the wire intersects this layer along a chord, and the length of the beam-heated segment is larger here than during the intersection along the diameter; therefore, the temperature spread is less pronounced.

Figure 7 shows the results from beam-profile measurements performed by both methods in the following gun operating mode: $U_{cath} = -1$ kV, $U_{contr} = 400$ V, and beam current $J_e = 0.17$ A. The coordinates of the beam's center are $x = 0$ and $y = 0$; the wire was tensioned in parallel to the X axis and moved stepwise along the Y axis. Shown are $q(x, 0)$, the emitted-power density profile along the wire that intersects the beam along its diameter, and $q(0, y)$, the emitted-power density profile along the Y axis obtained by sampling signals with coordinate $x = 0$ from a series of wire displacements transversely to the beam. Beam-current density profile $j(r)$, also shown in Fig. 7, was obtained from measurements of the current to the wire being displaced stepwise transversely to the beam.

Figure 8a shows the temperature profiles that are solutions to Eq. (2) for a long wire uniformly heated on a length $-x_0 \le x \le x_0$ by a beam with power density $Q_0 = 50$ W/cm^2. The effect of the wire heating by current J_h is considered.

Figure 8b shows signals from the photodetector, which according to the calibration in Fig. 3 would correspond to the measured temperature profiles. The signals thus obtained can be compared to those obtained in measurements along the diameter of a flat beam of radius $R = 1.5$ cm and measurements of a hollow (tubular) beam of radius $R = 1.5$ cm and thickness $\delta R = 0.3$ cm along the diameter $2x_0 = 0.3$ cm and an exterior chord $2x_0 = 0.6$ cm.

It follows from these graphs that, in order to determine the beam-power density profile from Eq. (2) using measured dependence $S(x)$, only measurements with the wire heating are acceptable. In fact, for a strong temperature dependence of the photodetector signal, on the assumption that the total wire length is finite ($L = 10$ cm),

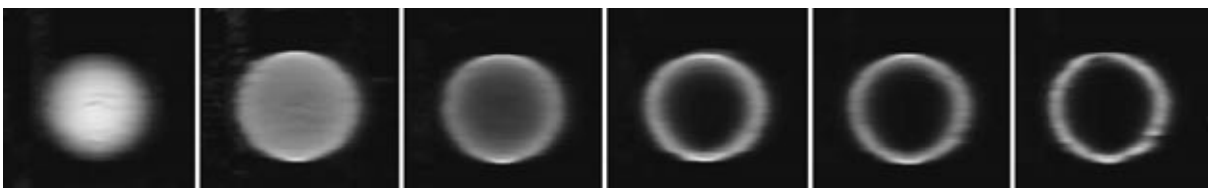

Fig. 6. Distribution of the emitted-power density during scanning of the beams formed at different voltages U_{contr} at the gun's control electrode (from left to right): 0, 100, 200, 350, 400, and 600 V.

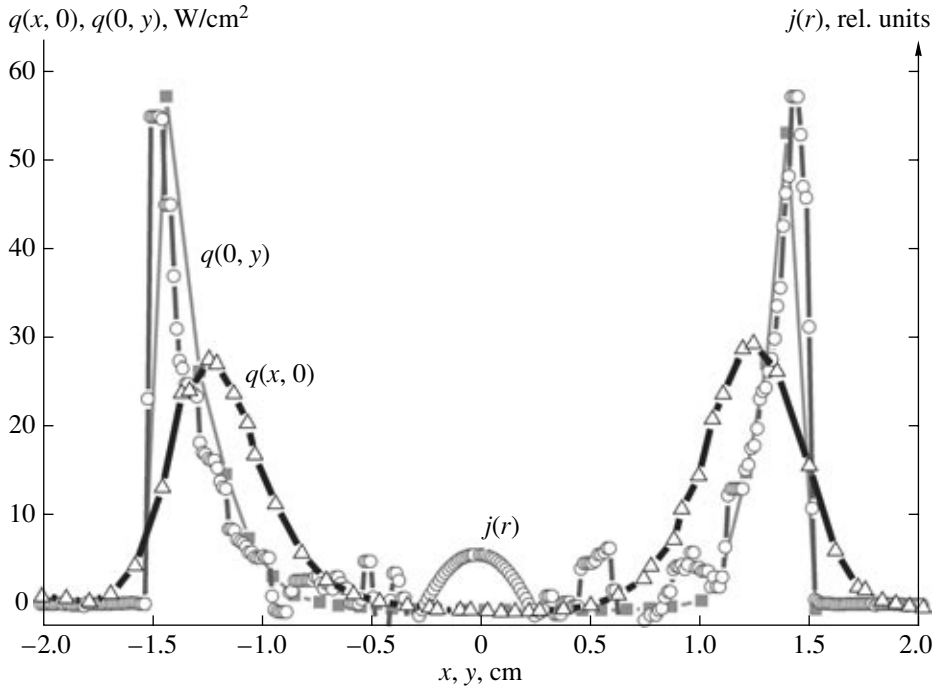

Fig. 7. Distribution of the emitted-power density along two mutually perpendicular beam diameters: $q(x, 0)$ along the wire and $q(0, y)$ along the line of wire movement; $j(r)$ is the beam-current density distribution.

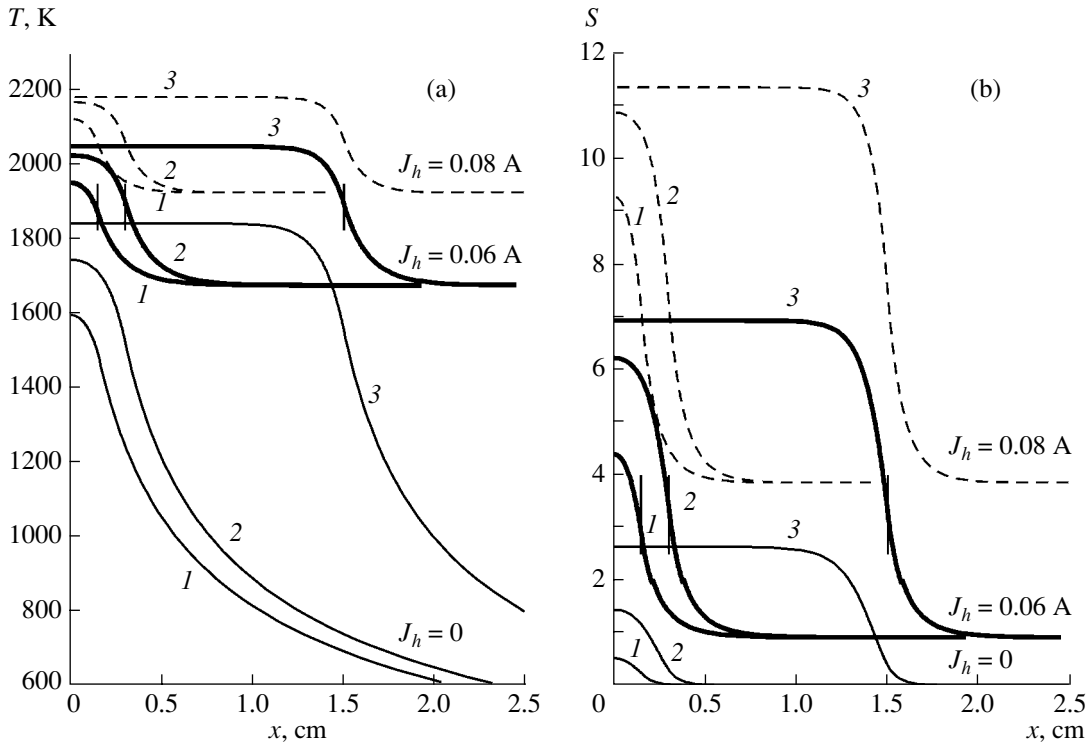

Fig. 8. (a) Temperature profiles and (b) photodetector signals during the wire heating by beam current J_h (figures near the curves) with power density $Q_0 = 50$ W/cm^2. In each measurement run, the beam heats the wire on length $2x_0 = 3$ cm (*1*), 0.6 cm (*2*), and 0.3 cm (*3*).

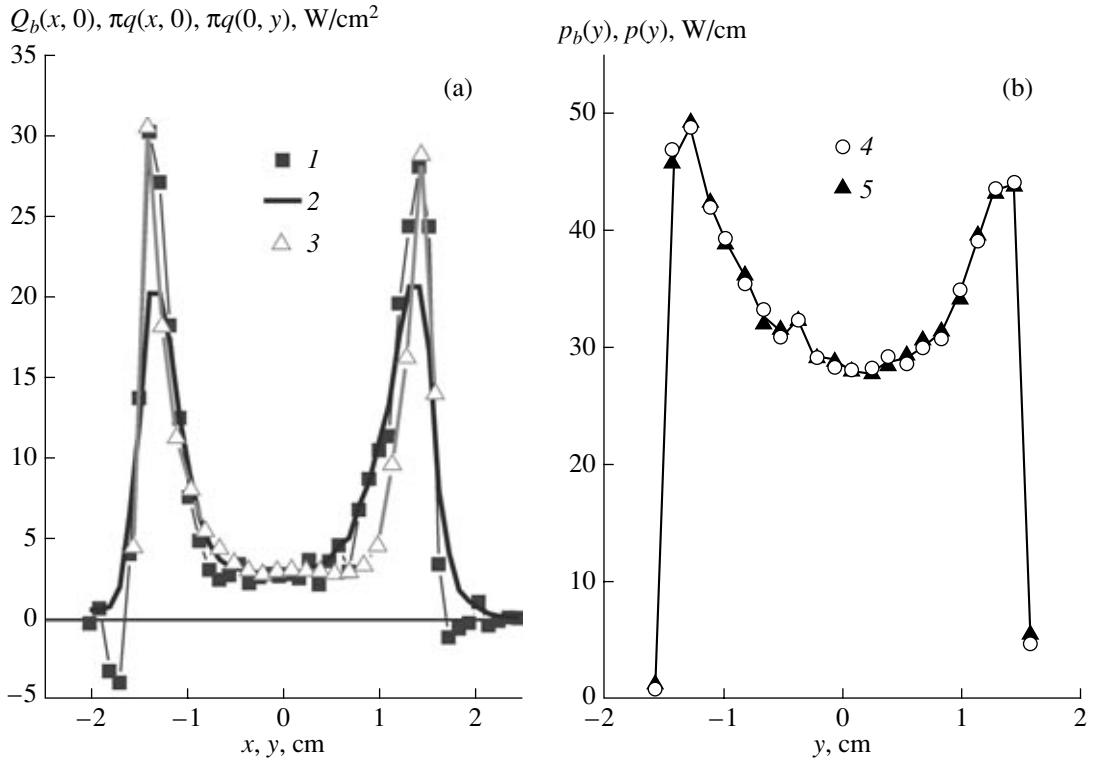

Fig. 9. (a) Power-density profiles in cross sections through the beam's center: (*1*) $Q_b(x, 0)$ for the beam, (*2*) $\pi q(x, 0)$ for the emission along the wire, (*3*) $\pi q(0, y)$ for the emission transversely to the wire; (b) integrals (*4*) $p_b(y_i)$ and (*5*) $p(y_i)$ along chords with coordinates y_i transverse to the beam.

adequate values of both the signal and characteristic linear dimensions of signal and temperature changes can be obtained only during heating. As is seen, filament current $J_h = 0.06$ A is close to the optimal value.

Figure 9 shows the results obtained during scanning of a tubular beam by the heated wire. The wire filament current $J_h = 0.05$ A. The average beam power is 220 W, the pulse beam current is ~1.9 A, the collector current

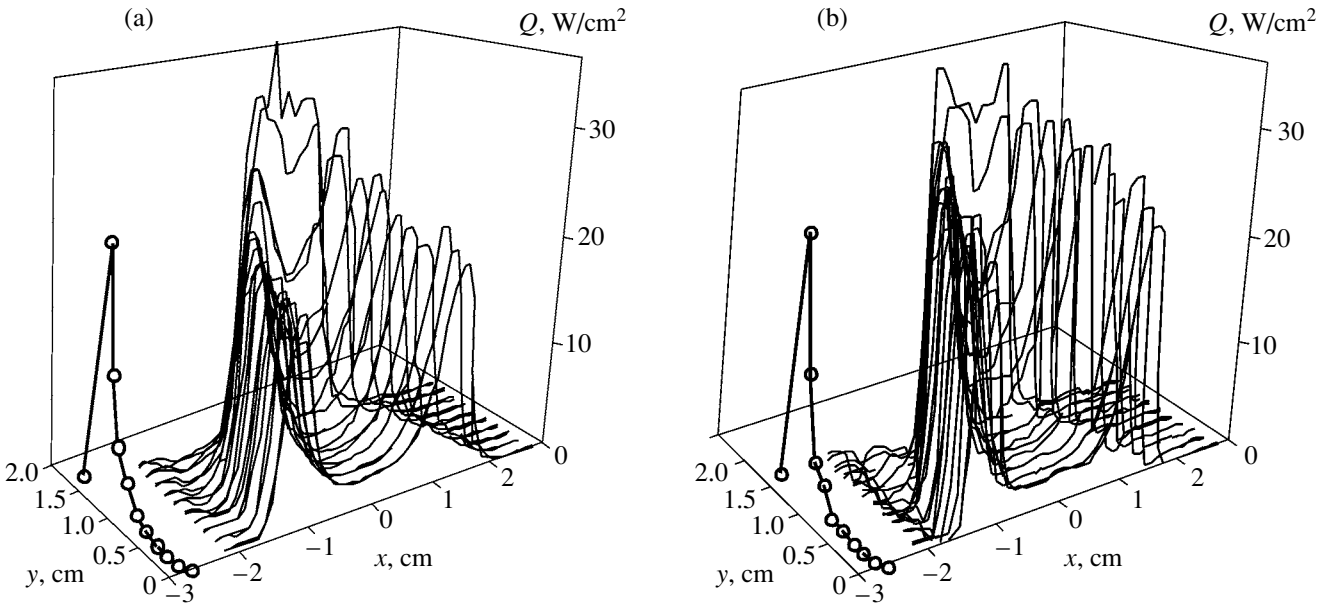

Fig. 10. Beam-power density profiles $Q(x)$ reconstructed from signal profiles $S(x)$ measured by scanning: (a) without and (b) with consideration for the left-hand side of Eq. (2). The beam profile in cross section $X = 0$ is plotted in the YZ plane (in the left part).

is 44 mA (at an off-duty factor of 43), and the electron energy is 5 keV. Figure 9a shows beam-power density profile $Q_b(x, 0)$ along its diameter and emitted-power density profile $\pi q(x, 0)$ minus the fraction of radiation due to filament current J_h. These profiles were found using signal $S(x, 0)$ picked off the wire that ran along the beam diameter, calibrations $T(S)$ and $q(S)$, Eq. (2), and reference dependences for $\rho(T)$ and $\chi(T)$. The wire was moved transversely to the beam with a 0.15-cm step. Photodetector signals $S(x, y_i)$ were measured in 20 positions. Emitted-power density profile $\pi q(0, y)$ obtained from signal sample $S(0, y_i)$ in the cross section through the beam's center, from which the fraction of radiation due to the filament current was subtracted, is shown for comparison.

Figure 9b shows integrals $p_b(y_i) = \int Q_b(x, y_i)dx$ and $p(y_i) = \pi \int q(x, y_i)dx$ along chords with coordinates y_i transversely to the beam. Their values coincide with a good accuracy. This means that the wire-absorbed beam power is emitted but is not transferred along the wire to the supporting frame.

Figure 10 shows the beam-power density distribution during the profile reconstruction with and without consideration for the thermal conductivity. As is seen, if the left-hand side of Eq. (2) is considered, the reconstructed profile becomes more uniform along the Y coordinate (Fig. 10b). The beam profile in cross section $X = 0$ is plotted in the YZ plane (in the left part of Fig. 10).

CONCLUSIONS

Measurements performed with a wire enabled the adequate experimental determination of the beam profile. Measuring the current through the wire with allowance for the emission distribution along the wire permitted reliable data on the beam profile to be obtained. The measured profiles agree well with the results of numerical calculations. The method described allows absolute density measurements of intense electron beams to be performed. Electron guns with a design described above were mounted on EC-35, EC-300 (Institute of Modern Physics, Lan'chzhou, China), and LEIR (CERN, Switzerland) electron-cooling facilities. Electron-beam profiles measured in various operating modes of the electron gun are the data necessary for its subsequent operation.

REFERENCES

1. Parkhomchuk, V.V. and Skrinsky, A.N., *Physics—Uspekhi*, 2002, vol. 43, no. 5. p. 473.
2. Budker, G.I., Dikansky, N.S., *et al.*, *Proc. IV All-Union Meeting on Accelerators of Charged Particles (Moscow, 1974)*, Moscow: Nauka, 1974, vol. 2, p. 309, *IEEE Trans. Nucl. Sci*., 1975, vol. VS-22, p. 2093.
3. Bublei, A., Goncharov, A., Ivanov, A., *et al.*, *Proc. of EPAC*, Paris, France, 2002, p. 1357.
4. Bubley, A.V., Parkhomchuk, V.V., and Reva, V.B., *International Workshop on Beam Cooling and Related Topics (ECOOL-2003) RIKEN*, Japan, 2003.
5. Konstantinov, S.G., Parkhomchuk, V.V., and Reva, V.B., *Zh. Tekh. Fiz.*, 2003, vol. 73, no. 1, p. 91.
6. Espe, V., *Tekhnologiya elektrovakuumnykh materialov. T. 1. Metally i materialy s metallicheskoi provodimost'yu* (Technology of Electric Vacuum Materials. vol. 1, Metals and Materials with Metallic Conduction), Moscow: GEI, 1962.